Numerical investigation of thermo-hydraulic performance in an annular heat exchanger with sinusoidal vortex generators

Yanru Wang[1] · Cheen Sean Oon[1] · Ji-Jinn Foo[1] · Manh-Vu Tran[1] · Sayshar Ram Nair[1] · Foo Wah Low[2]

Abstract

This study investigates thermal performance enhancement by utilizing vortex generators (VGs). VGs come in many designs, and this paper proposes optimizations for the sinusoidal vortex generator (SVG) when used in an annular conduit to improve heat transfer with minimal pressure drop. Two vital parameters of the SVG are analyzed, namely, blockage ratios (BRs) (0.1 and 0.2) and attack angles (α) (0–90°). The investigated fluid regime is turbulent, with the Reynolds number (Re) ranging from 5973 to 11,947. Three rows of SVGs are fitted on the surface of the inner pipe, where constant heat flux is applied, while the outer pipe wall is entirely insulated. The results indicate that the highest Nusselt number is enhanced by 20.4% over the smooth pipe when the case with $BR = 0.2$ and $\alpha = 90°$ is used at $Re = 5973$. However, the friction factor increases by 56.5% for the same case. Two types of transverse vortices are identified, where one type has its rotational axis normal to the inner pipe surface, and the other has its rotational axis parallel to the inner pipe surface. Those vortices with the axis perpendicular to the pipe surface merge with the fluid above the SVG to develop longitudinal vortices in different BRs and α. The case with $BR = 0.2$ and $\alpha = 15°$ yields the greatest average performance evaluation criterion (PEC) compared to other tested cases with a value of 1.054. This study finds that SVGs can contribute to a more efficient annular pipe-based heat transfer system.

Keywords Annular conduit · Heat exchanger · Sinusoidal vortex generators · Thermo-hydraulic performance · Turbulent flow

Abbreviations

BR	Blockage ratio
DPHE	Double-pipe heat exchanger
DW	Distilled water
Nu	Nusselt number
PEC	Performance evaluation criterion
Re	Reynolds number
SST	Shear stress transport
SVG	Sinusoidal vortex generator
VG	Vortex generator

List of symbols

α	Attack angle
f	Friction factor
$\overline{h}$	Average heat transfer coefficient (W m^{-2}K^{-1})
q	Heat flux (W m^{-2})
$\overline{T}_s$	Average inner wall temperature (°C)
T_b	Fluid bulk temperature (°C)
D_h	Hydraulic diameter (mm)
k	Thermal conductivity (W m K^{-1})
ρ	Density (kg m^{-3})
v	Velocity (m s^{-1})
μ	Viscosity (Pas)
ΔP	Pressure drop (Pa)
L	Length (m)
Pr	Prandtl number
a	Ratio of the outer diameter of the inner tube over the inner diameter of the outer tube
x	Flow direction (m)

Subscripts

s	Smooth pipe
ann	Annular conduit

✉ Cheen Sean Oon
  oon.cheensean@monash.edu; oonsean2280@yahoo.com

1 Mechanical Engineering Discipline, School of Engineering, Monash University, 47500 Bandar Sunway, Malaysia

2 Department of Electrical and Electronic Engineering, Lee Kong Chian Faculty of Engineering and Science, Universiti Tunku Abdul Rahman, Bandar Sungai Long, 43000 Kajang, Selangor, Malaysia

Introduction

The double-pipe heat exchanger (DPHE) consists of two concentric pipes, where one fluid flows within the inner pipe while another fluid flows in the annular space between the inner and outer pipes. DPHEs have been utilized in various industries due to their relatively simple design, which includes air conditioning and refrigeration, waste heat recovery, and food production. When the heat transfer efficiency of DPHEs is enhanced with fins, large-scale applications like power plants can be viable as the hot exhaust gases can be more efficiently utilized to heat the cold fluid through the device [1]. Many approaches can be taken to improve the thermal performance of DPHEs. One such way is applying a fluid with better thermophysical properties, which include phase change materials and nanofluids [2, 3]. On the other hand, fins, inserts, or vortex generators (VGs) could also be used to improve the overall heat transfer performance [4]. Meanwhile, to evaluate the thermo-hydraulic performance of the enhanced geometry with fins or VGs, the performance evaluation criterion (PEC) proposed by Webb [5] in 1981 can be used. The PEC is defined as the ratio of the Nusselt number enhancement to friction factor enhancement resulting from VGs or other enhancements. A higher PEC value corresponds to a higher heat transfer generated with a lesser increase in pressure drop. Thus, less pumping power was required to achieve the same heat transfer with a smaller equipment size.

VGs have been widely investigated in different heat exchangers due to their outstanding thermal performance. There are two patterns of VGs, namely, longitudinal VGs and transverse VGs. Longitudinal VGs, including wings, winglets, or winglet pairs, could generate longitudinal vortices, where fluid is strongly mixed without obstructing the main flow. Whereas transverse VGs, such as baffles or circular fins, generate transverse vortices that create a significant pressure drop in the recirculation zone area. Longitudinal vortices could enhance heat transfer globally and locally, while transverse vortices only improve local heat transfer [6]. Therefore, longitudinal vortices are more effective and preferable in improving heat transfer compared to the transverse vortices.

Some researchers have explored the thermal performance of various VGs in the annular tube of double-pipe heat exchangers. The studies aimed to achieve maximum heat transfer by combining VG with other fins or applying VG individually. For example, Arjmandi et al. [7] investigated the simultaneous use of VGs and twisted tape in the annular tube of a DPHE with various pitch ratios of 0.09–0.18 and angles of 0°–30°. They discovered that the pitch ratios were critical in affecting the heat exchanger

efficiency, with the best geometry obtained at the pitch ratio of 0.18, angle of 30°, and Reynolds number (Re) of 20,000. Zhang et al. proposed various VGs in the helical annular passage, such as triangular winglet pair VGs [8], delta and rectangular wing/winglet pair VGs [9], and streamlined winglet pair VGs [10]. They concluded that streamlined winglet pair VGs could achieve the highest PEC value among all the tested designs. The optimal case depended on the Re range, the height, the number of VG, and the attack angle (α) of the streamlined winglet pair VGs. Mousavi et al. [11] reported on the findings of the airfoil-shaped VGs with different thicknesses of 0.21–0.3 mm and pitch ratios of 2.9–6.78 in a double-pipe heat exchanger. The results showed that the highest PEC value was 1.91 with a geometry thickness of 0.3 mm, pitch ratio of 2.9, and Re of 6000. This was the highest found when comparing the results with other studies. Maakoul et al. [12] carried out a numerical investigation of helical fins with different fin spacings ranging from 50 to 200 mm on the annular side of the double-pipe heat exchanger. The best average PEC found was 1.06 at the fin spacing of 0.1 using helical fins in place of longitudinal fins. Wang et al. [13] investigated the staggered helical fins with various torsion angles and fin numbers in a double-pipe heat exchanger. The results indicated that the pressure drop was significantly reduced, and the overall performance was enhanced by 10–30% compared to the traditional helical fins. Bai et al. [14] investigated three densely longitudinal fins, including arc-shaped fins, folded fins, and long straight fins mounted in an annular heat exchanger. The short arc-shaped and fold fins enhanced the Nusselt number by 35 and 27%, respectively, compared to the straight fins. However, severe flow separations in the flow resulting in the friction factor increase by 2209 and 1088%, respectively. Nair et al. [15] explored the influence of rectangular swirl-inducing fins with angles 10°–40° in an annular heat exchanger. They found that the 30° angled fin could not increase heat transfer because of the tiny longitudinal vortices tracing the heat in the near wall region, while the 40° fin achieved the highest heat transfer. Wang et al. [16] analyzed perforated curve fins with different hole numbers 0–16 in an annular passage. This design showed the PEC higher than 1 when the Re was lower than 4277, while the enhanced heat transfer could not comprise the improved pressure drop at higher Re ranges.

Various vortex generators have been investigated for use in circular pipes, including delta wing/winglets [17–23], delta winglet pairs [24], rectangular winglets [25, 26], and other novel types [27–36] such as elliptical insert, sinusoidal ribs, louvered V-winglet, conical strip, and longitudinal swirl generators. Pourhedayat et al. [20] reported a new arrangement of triangular winglets in a circular channel and analyzed various parameters, such

as longitudinal and latitudinal pitches, angle of winglets, winglet arrangement, and aspect ratio. The heat transfer rate was enhanced using the forward configuration and reducing the longitudinal pitch and aspect ratio. Moreover, the latitudinal pitch of 20 mm achieved the best thermal performance among all test cases, with pitch values ranging from 0 to 40 mm. Liu et al. [25] explored the thermal behavior of rectangular winglet VGs in circular pipes with Res ranging from 5000 to 17,000. Increasing the slant angle or winglet height enhanced the Nusselt number and friction factor. However, the PEC value was raised and then reduced with the increasing slant angle and winglet height. The PEC value was more than 1 if the Re was less than 8000. Abdelmaksoud et al. [27] compared the heat transfer performance of various VG designs (straight, triple-curved, and double-curved) in circular tubes. The thermal performance was increased when reducing the pitch ratios from 5 to 2. Triple-curved vortex generators achieved the highest PEC value compared to other designs, whereas the PEC was less than 1 in turbulent regions when the Re was higher than 6000. Chokphoemphun et al. [28] investigated the influence of winglet VGs on heat transfer performance with an α of 30° in a circular tube. They observed that the Nusselt number and friction factor enhanced with the increase in the blockage ratio (BR) but decreased with the reduction of the pitch ratio. PEC values of 1.35–1.59 were obtained by applying winglet VGs with Re ranging from 5300 to 24,000. Du et al. [29] employed sinusoidal ribs in a circular tube with laminar flows. They analyzed different rib heights, amplitudes, widths, numbers, and pitches and concluded that the PEC value was enhanced by raising rib height but reducing rib amplitude, width, and pitch. Moreover, raising the number of ribs from 1 to 3 increased the PEC value, while increasing the numbers beyond 3 had the opposite effect.

Based on the literature review, the previous studies have extensively examined flat surface vortex generators but have found them to produce limited vortices. Generating multiple vortices from a single VG is crucial for improving local and global fluid mixing. Therefore, this paper introduces the sinusoidal vortex generator (SVG) fitted in an annular conduit. The unique sinusoidal shape is expected to generate more vortices than the flat surface. This study investigates the influence of vortices induced by the SVG in a detailed way. Additionally, the α and BR are investigated for the SVG to maximize heat transfer performance while minimizing the impact of pressure drop increase. Furthermore, the thermo-hydraulic performances of different SVG configurations are evaluated under turbulent flow conditions. This investigation strives to design a more efficient annular pipe-based heat transfer system.

Methodology

Geometry design

As shown in Fig. 1a, the entire length of the annular conduit is 1.5 m. Three zones of SVGs are equipped along the inner pipe wall with an interval of 300 mm. The inner pipe wall is subjected to a continuous heat flux of 38,346 W m^{-2} at the mid-section for 1200 mm (150 mm at the beginning and ending are insulated), while the outer wall is completely insulated. Only the turbulent fluid domain is considered in this study, where the volume flow rate varies from 10 to 20 L min^{-1}, corresponding to the Re ranging from 5973 to 11,947. Figure 1b displays the dimensions of the SVG with BR = 0.1 and α = 45°. The BR is defined as the height of the SVG relative to the hydraulic diameter of the annular channel, while the α is the angle between the flow direction and the centerline of the SVG. A circular ring with a width of 8 mm and a thickness of 0.5 mm supports the SVG. Four SVGs are placed symmetrically in a counter-rotated direction with α ranging from 0° to 90°. Two BRs of 0.1 and 0.2 are studied with different SVG heights. The sinusoidal shape of the SVG, created with an amplitude of 1 mm, enhances the turbulence in the fluid flow compared to a flat surface type VG. The displacement between the leading edges of two SVGs changes with different α, ranging from 3.43 to 9.21 mm, leaving enough space between the opposing SVGs to develop the longitudinal vortices at α = 90°. Moreover, although the circular ring causes an additional pressure drop, it is negligible due to its small thickness. This study aims to identify the optimal α and BR for the best PEC when using SVGs in an annular heat exchanger. Distilled water (DW) as the cooling fluid passes the annular channel with an inlet temperature of 20 °C. The boundary conditions are summarized in Table 1.

Numerical methods

Three-dimensional steady-state flow in the annular passage is analyzed by ANSYS Fluent. Conservation equations for the steady turbulent flow are described from Eqs. (1) to (3) [14].
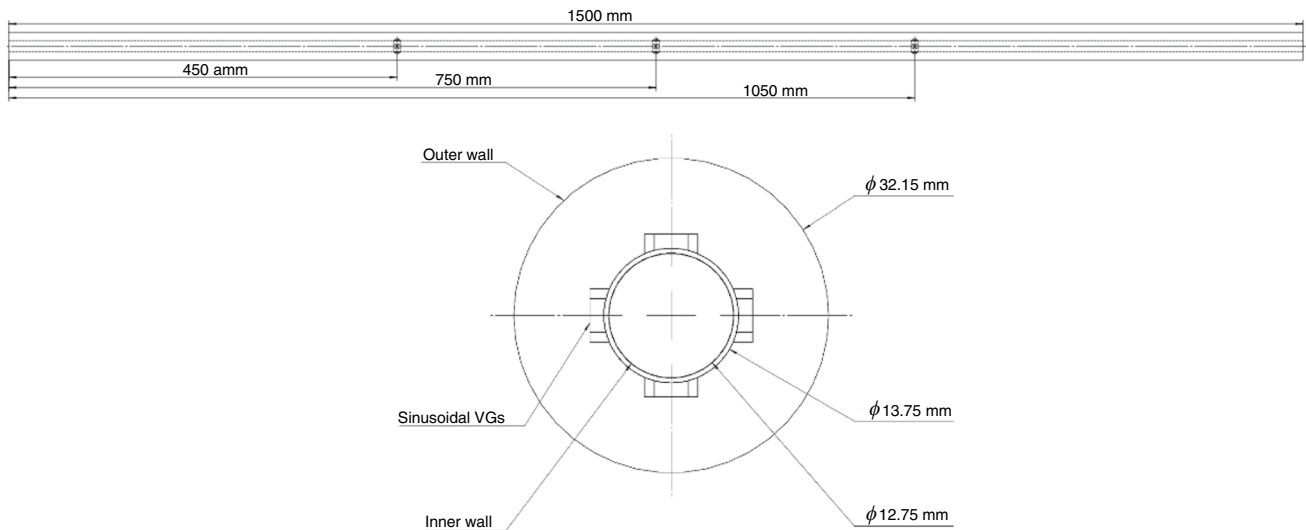
Continuity equation:

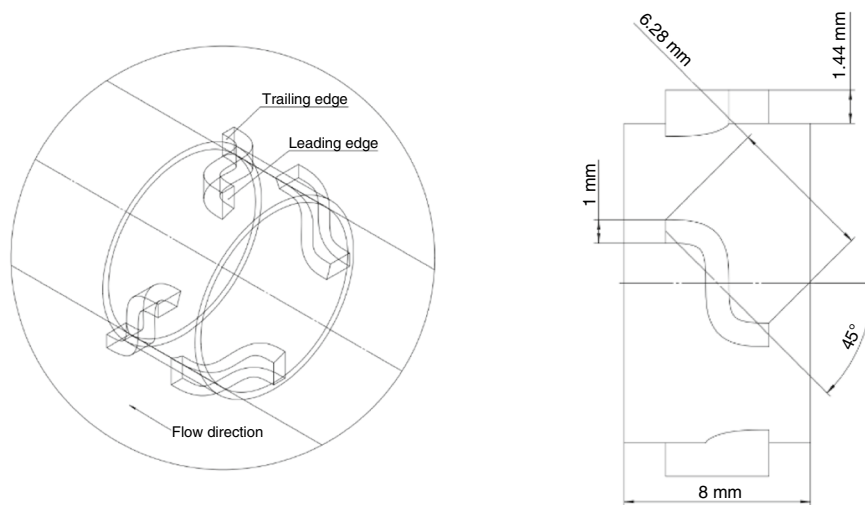$$\frac{\partial}{\partial x_{\mathrm{i}}}\left(\rho \mu_{\mathrm{i}}\right) = 0 \tag{1}$$

Momentum equation:

$$\frac{\partial}{\partial x_{\mathrm{j}}}\left(\rho \mu_{\mathrm{i}} \mu_{\mathrm{j}}\right) = -\frac{\partial P}{\partial x_{\mathrm{i}}} + \frac{\partial}{\partial x_{\mathrm{j}}}\left[\mu\left(\frac{\partial \mu_{\mathrm{i}}}{\partial x_{\mathrm{j}}} + \frac{\partial \mu_{\mathrm{j}}}{\partial x_{\mathrm{i}}}\right)\right] + \frac{\partial}{\partial x_{\mathrm{j}}}\left(-\rho \overline{u_{\mathrm{i}}' u_{\mathrm{j}}'}\right) \tag{2}$$

Energy equation:

(a) Annular conduit with SVGs

(b) SVGs with BR=0.1 and α=45°

Fig. 1 Dimensions of **a** annular conduit with SVGs and **b** SVGs with BR = 0.1 and $\alpha = 45°$

Table 1 Summary of boundary conditions applied for all the simulations

Parameter	Boundary condition
Inlet	Velocity inlet
Outlet	Pressure out
Inner pipe wall	Constant heat flux (38,346 W m^{-2})
Outer pipe wall	Fully insulated
Inlet fluid temperature	20 °C
SVG	Conductive
Re	5973–11,947

$$\frac{\partial}{\partial x_{\mathrm{i}}}\left(\rho\mu_{\mathrm{i}}T\right) = \frac{\partial}{\partial x_{\mathrm{j}}}\left[\left(\frac{\mu}{\mathrm{Pr}} + \frac{\mu_t}{\mathrm{Pr}_t}\right)\frac{\partial T}{\partial x_{\mathrm{j}}}\right] \tag{3}$$

The thermophysical properties of the DW shown in Table 2 are constant due to the negligible variations in fluid temperature. Gravity is not included in this study. The shear stress transport (SST) k–ω model is utilized, where the simulation grid cell has a first layer thickness of 0.028 mm to ensure that the dimensionless wall distance $y+$ is lower or equal to 1. Combining the chosen turbulence model and grid with strict $y+$ consideration ensures that the generation of vortices from the SVG is as accurate as possible with reasonable computational resource requirements. The coupled algorithm is used for coupling the velocity–pressure

Table 2 Thermophysical properties of the DW at 20 °C [37]

Properties	DW
Thermal conductivity /W m K^{-1}	0.6024
Viscosity /Pas	0.00079
Specific heat capacity /J kg^{-1} K^{-1}	4182
Density /kg m^{-3}	998.5

field, as it is robust to converge for addressing the complex geometries. The second-order upwind scheme is applied to discretize all equations to achieve more precise results than the first-order upwind scheme. The simulation is terminated once the residuals for the continuity, velocities, energy, k, and ω are below 10^{-6}.

The grid independence study is implemented to study the variations in Nusselt number regarding the mesh element number and quality. The method used is based on the methodology by Roache et al. [38] to determine the Richardson extrapolate. The annular conduit with SVGs at $\alpha = 90°$ and BR = 0.1 is selected for the mesh independence study at Re = 11,947.

Figure 2 shows that tetrahedral meshes are used for all domains with eight inflation layers set for the inner wall, outer wall, and VG regions with a growth rate of 1.2. The course, medium, and fine mesh are used with the number of elements 2,830,748, 6,872,857, and 12,676,788, respectively. The average Nusselt number difference between the course and medium mesh is found to be 12.45%, while it reduces to 2.69% when refining the mesh to the fine level. Therefore, the medium mesh is selected to simulate all cases to minimize computational costs while ensuring reasonably accurate results.

Parameter definitions

This section includes all equations used for evaluating the thermal performance of annular conduits with various SVG designs.
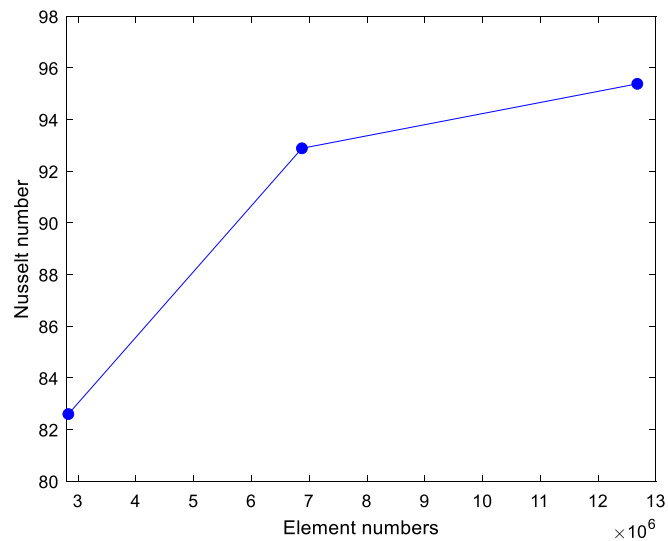
Equation (4) defines the average heat transfer coefficient.

$$\bar{h} = \frac{q}{\left(\overline{T_s} - T_b \right)} \tag{4}$$

Fig. 2 Grid independence study **a** mesh in the fluid computational domain and **b** Nusselt number variations versus element numbers in the annular conduit with SVGs at BR = 0.1, $\alpha = 90°$, and Re = 11,947
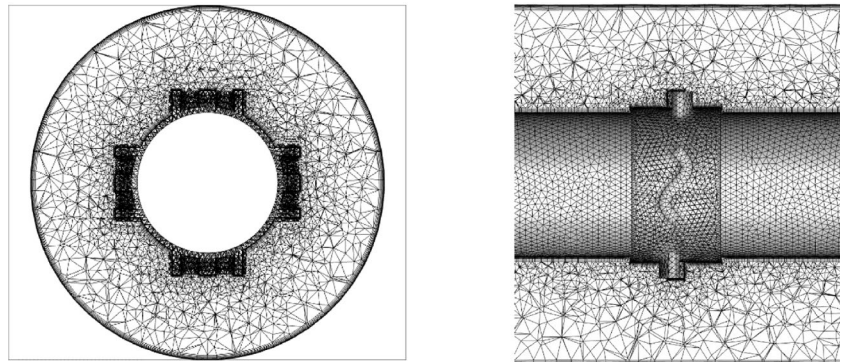
(a) Mesh in the computational domain

(b) Nusselt number variations in the conduit with SVGs

Equation (5) defines the average Nusselt number.

$$\overline{Nu} = \frac{\overline{h}D_h}{k} \tag{5}$$

Equation (6) defines the Reynolds number.

$$Re = \frac{\rho v D_h}{\mu} \tag{6}$$

Equation (7) defines the friction factor.

$$f = \frac{2\Delta P D_h}{L\rho v^2} \tag{7}$$

Equation (8) defines the PEC value [13].

$$PEC = \frac{Nu}{Nu_s} / \left(\frac{f}{f_s}\right)^{1/3} \tag{8}$$

To validate the accuracy of the simulation results, Gnielinski and Petukhov equations are employed in Eqs. (9) and (14), respectively, to validate the Nusselt number [39, 40]. At the same time, the friction factor is validated by Petukhov and Blasius equations shown in Eqs. (15) and (16), respectively [31]. These equations are suitable for turbulent flows.

$$Nu = \frac{\left(\frac{f_{ann}}{8}\right)Re\,Pr}{k_1 + 12.7\sqrt{\frac{f_{ann}}{8}\left(Pr^{\frac{2}{3}}-1\right)}} \left[1 + \left(\frac{d_h}{L}\right)^{\frac{2}{3}}\right] F_{ann}K \tag{9}$$

where the parameters used for Gnielinski correlation are defined in Eqs. (10)–(13).

$$k_1 = 1.07 + \frac{900}{Re} - \frac{0.63}{(1 + 10\,Pr)} \tag{10}$$

$$f_{ann} = \left(1.8\log_{10} Re^* - 1.5\right)^{-2} \tag{11}$$

$$Re^* = Re\frac{\left(1 + a^2\right)\ln a + \left(1 - a^2\right)}{(1 - a)^2 \ln a} \tag{12}$$

$$F_{ann} = 0.75a^{-0.17} \tag{13}$$

$$Nu = \frac{\left(\frac{f}{8}\right)Re\,Pr}{1.07 + 12.7\left(\frac{f}{8}\right)^{0.5}\left(Pr^{\frac{2}{3}}-1\right)} \tag{14}$$

f could be obtained by Eq. (15).

$$f = (0.79\ln(Re) - 1.64)^{-2} \tag{15}$$

$$f = 0.316 Re^{-0.25} \tag{16}$$

Validations

The simulation results of smooth annular pipe are validated by theoretical correlations. As described in Fig. 3, the deviations for the average Nusselt number between the simulation result and Petukhov and Gnielinski equations are 8.66 and 4.46%, respectively. Furthermore, the average friction factor

Fig. 3 Validations between the simulation results and theoretical corrections for smooth pipes
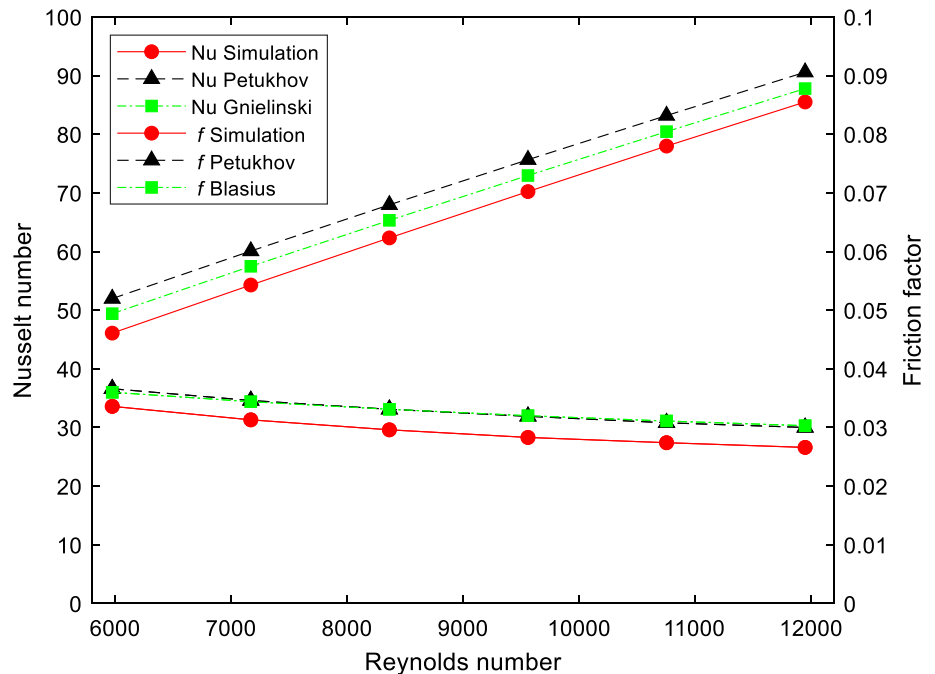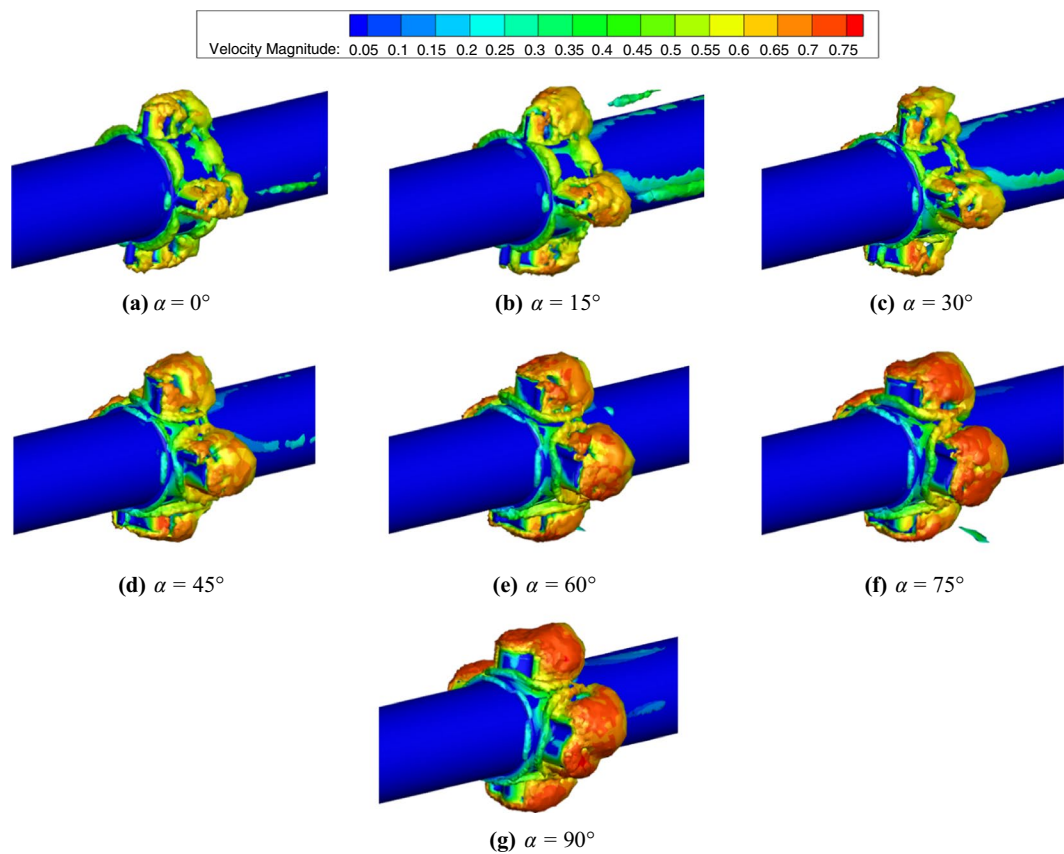
Fig. 4 Q criterion colored by the velocity magnitude in various conduits with BR = 0.2 and Re = 11,947

deviations for Petukhov and Blasius correlations are 11.51% and 11.46%, respectively. Therefore, the current numerical model can accurately estimate the heat transfer performance of the annular conduit for the various tested SVG designs.

Results and discussion

Fluid flow characteristics

Figure 4 shows the Q criterion iso-surface colored by the velocity magnitude of various conduits featuring a BR of 0.2 and Re of 11,947. Q criterion visualizes the vortical structures and flows turbulence intensity along the channel. In all cases, transverse and longitudinal vortices are present in the SVG regions. The transverse vortices form due to flow separation resulting from the sudden expansion of the channel, whereas the longitudinal vortices develop around the transverse vortices as the flow interacts with the SVG edges, as explained by the horseshoe phenomenon. These horseshoe vortices are more effective in cooling down the inner wall in the near-fin regions but diminish in strength as they move away from the SVG area due to reduced velocities.

Additionally, small vortices arise before the SVGs due to the sudden reduction of the flow channel. Increasing the α of the SVGs enhances flow velocities and leads to more powerful vortices initialized near the SVG zone. A weak vortex region is also found between two SVGs, with lower flow velocities than in other areas.

Velocity streamlines shown in the image on the left in Fig. 5 are from the transverse cross-section located 20 mm behind the SVG, while the image on the right presents the top view of the flow. At an α of 90°, the left image of Fig. 5g shows three different vortices that arise from a single SVG. Vortex A, originating from the leading edge, is less intense than the vortex C, formed at the trailing edge. Moreover, two counter-rotated transverse vortices are observed behind the VG in the right image of (g). These transverse vortices merge with the incoming flow above the VG, leading to fluid twisting and the development of a large longitudinal vortex B with its center positioned near the low-pressure zone of the leading-edge area. For $\alpha = 75°$, the longitudinal vortices generated by the trailing edges are slightly weaker than those at 90°. In addition, the transverse vortices with a similar size cause vortex B to separate into two longitudinal vortices with a counter-rotated direction. When α is reduced to 60°, the transverse vortices near the leading-edge flow area

Fig. 5 Streamlines in transverse planes in various conduits with BR = 0.1 and Re = 11,947


(a) $\alpha = 0°$

(b) $\alpha = 15°$

(c) $\alpha = 30°$
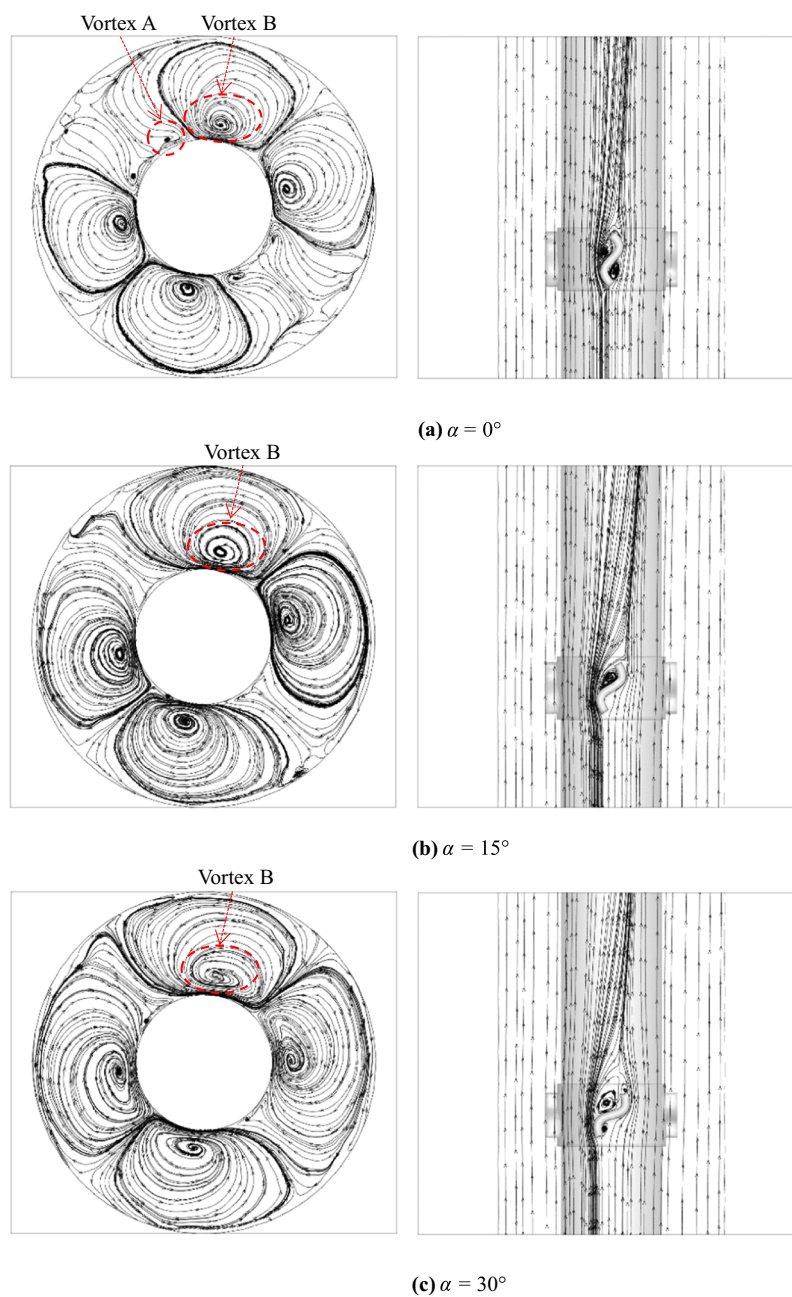
become stronger, shifting the longitudinal vortex center near the trailing vortex C. At $\alpha = 45°$, only one transverse vortex is observed in the flow. The increased displacement between two VGs results in the connection between the vortices B and C. If decreasing the α to 30° and 15°, the vortices caused by the trailing edges are completely absorbed by the powerful vortex B. The weakest vortices are observed at $\alpha = 0°$ with the tiny vortex A generated between the two vortices B. The sinusoidal curve results in the pressure difference in the two sides of the VG, where the twisting flow causes the generation of vortex B.

Figure 6 describes the velocity streamlines and pressure contours of the annular conduit with α of 0°, 45°, and 90° and BRs of 0.1 (left) and 0.2 (right). The pressure contour indicates a decrease in pressure as the flow passes through the SVG for all cases. The main fluid turns the direction to fill the gap between the SVG and the outer wall. The pressure drag is caused due to fluid separation caused by the sudden expansion of the channel. Subsequently, a secondary flow is observed after the SVG, which breaks the inner wall thermal boundary layer, leading to enhanced fluid mixing and high local heat transfer. Only small transverse vortices are found for all cases with a BR of 0.1. However, as the

Fig. 5 (continued)

(d) $\alpha = 45°$

(e) $\alpha = 60°$

(f) $\alpha = 75°$

(g) $\alpha = 90°$
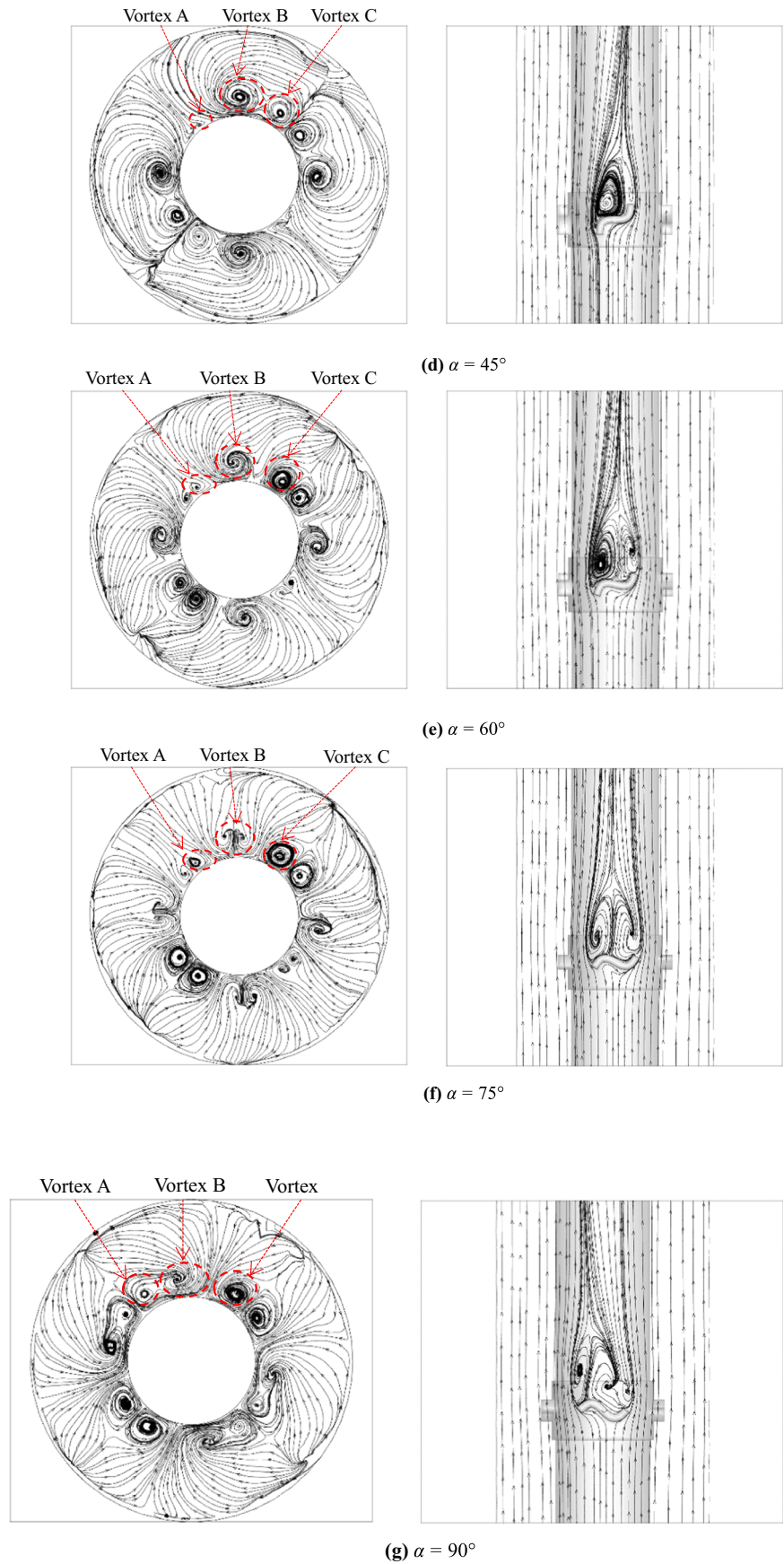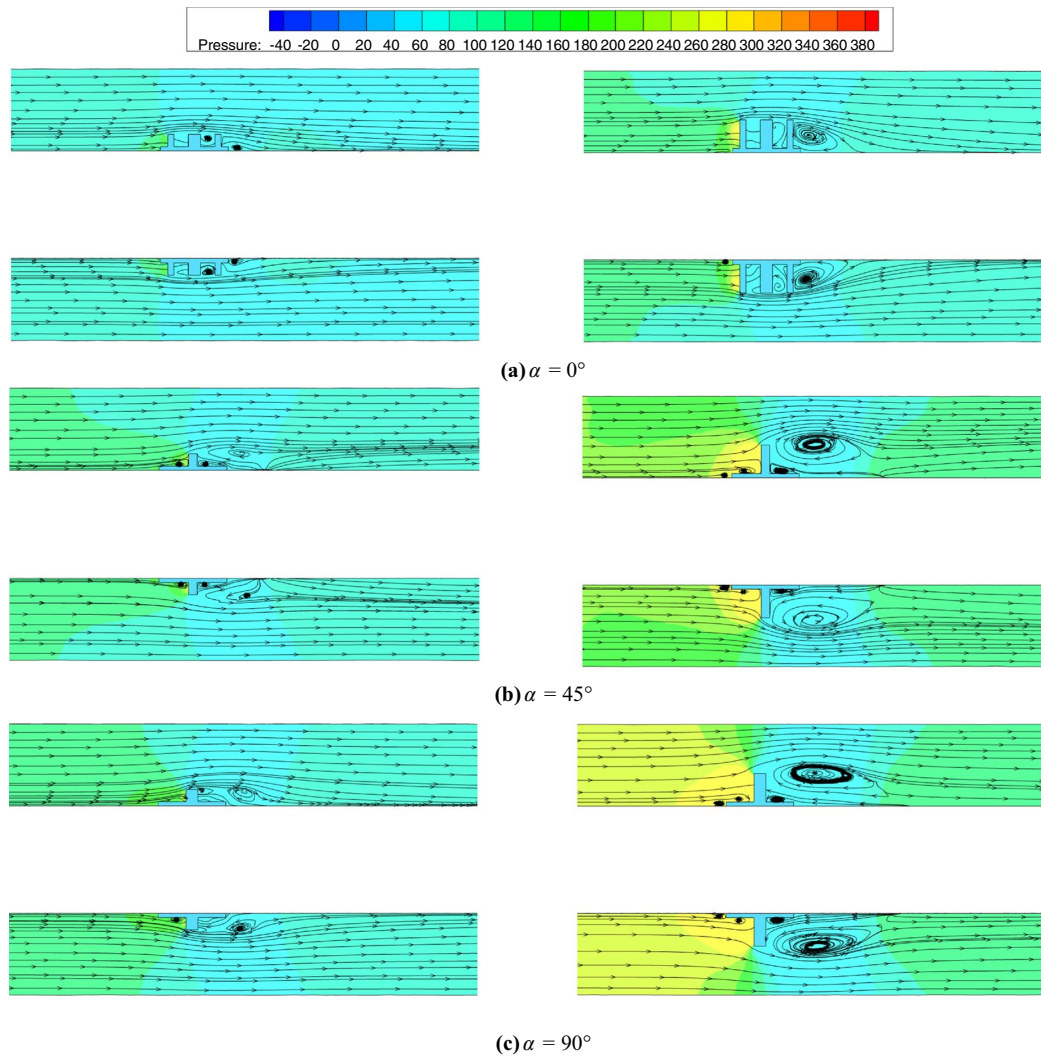
Fig. 6 Velocity streamline and pressure contour at BR=0.1 (left) and BR=0.2 (right) and Re=11,947 with different α **a** $\alpha=0°$, **b** $\alpha=45°$, and **c** $\alpha=90°$

SVGs height increases, more substantial fluid mixing and a larger recirculation zone are generated due to stronger flow separation. Furthermore, the pressure drop increases when either α or BR increases. The most significant pressure drop is observed for the case with BR=0.2 and $\alpha=90°$.

Effects of SVGs on Nusselt number

Figure 7 illustrates the Nusselt number variations for different annular conduits with their respective SVG design at different Res, BRs, and α. The heat transfer is generally improved when augmenting the BR from 0.1 to 0.2. For both BRs, the model with $\alpha=90°$ performs the best due to the strongest vortices observed in Fig. 4. When increasing the Re from 5973 to 11,947, the Nusselt number difference

between the low α cases and the 90° case reduces, except for the 0° case. For example, the 15° case shows the lowest Nusselt number among all the SVG cases at Re=5973 and BR=0.1, while it increases to the second highest value at Re=11,947. Hence, larger α can be used to achieve better Nusselt numbers at low Re, while smaller α cases are preferable for high Re. Moreover, the lowest Nusselt number is obtained at the 0° case among the enhanced designs due to the weakest vortices formed in the flow domain.

Figure 8 illustrates the Nusselt number enhancement of annular conduits with various SVGs compared to the plain tube. The results show that increasing the BR causes a further improvement in the Nusselt number for the same α. In addition, at Re=5973, the highest Nusselt number enhancement is obtained by 20.4% in the case with BR=0.2 and

Fig. 7 Nusselt number variations of various conduits with **a** BR = 0.1 and **b** BR = 0.2

(a) BR = 0.1

(b) BR = 0.2
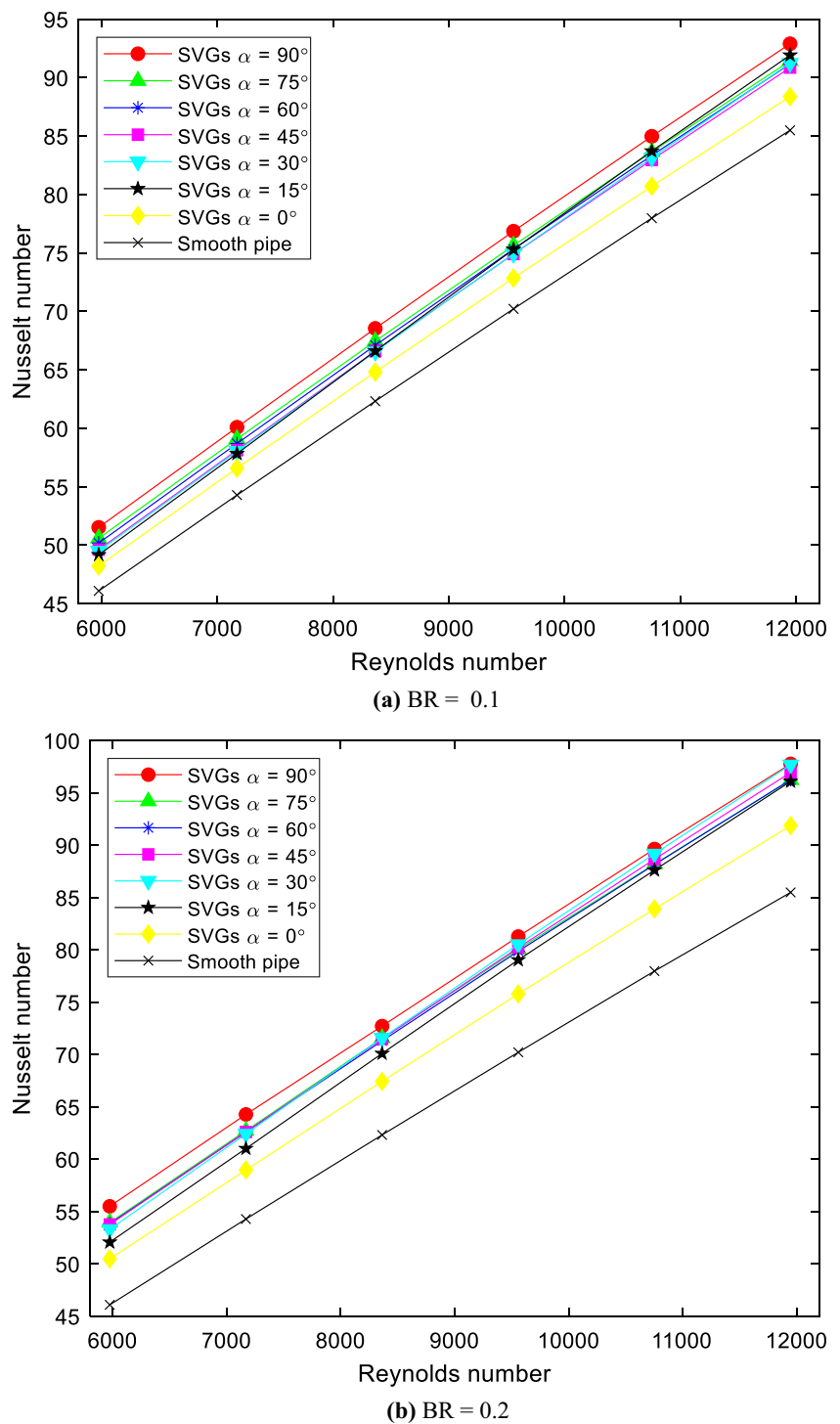
$\alpha = 90°$, while it only improves by 4.6% in the case with BR = 0.1 and $\alpha = 0°$. The augmentation of the Nusselt number is more significant at low Re, gradually decreasing with the increasing Re. However, the Nu/Nu$_s$ ratio increases as Re rises for the 15° case with BR = 0.1. It indicates that a low α with low BR is effective in enhancing heat transfer at high Re, where the generated vortices in the flow can cause higher heat transfer improvement compared to that at low

Re. About 15° and 30° cases display a similar trend for Nu/Nu$_s$ ratio as the vortex patterns are similar for both cases, which are observed in Fig. 5. As Re increases, the small vortices generated by the SVG at larger α are not efficiently improving heat transfer as well as the large vortices. Therefore, Nu/Nu$_s$ decreases for these SVG cases with larger α. In addition, the Nusselt number is enhanced by 3.4% for the model with BR = 0.1, $\alpha = 0°$, and Re = 11,947 compared to

**Fig. 8** Nusselt number enhancement of various conduits with **a** BR = 0.1 and **b** BR = 0.2

(a) BR = 0.1

(b) BR = 0.2
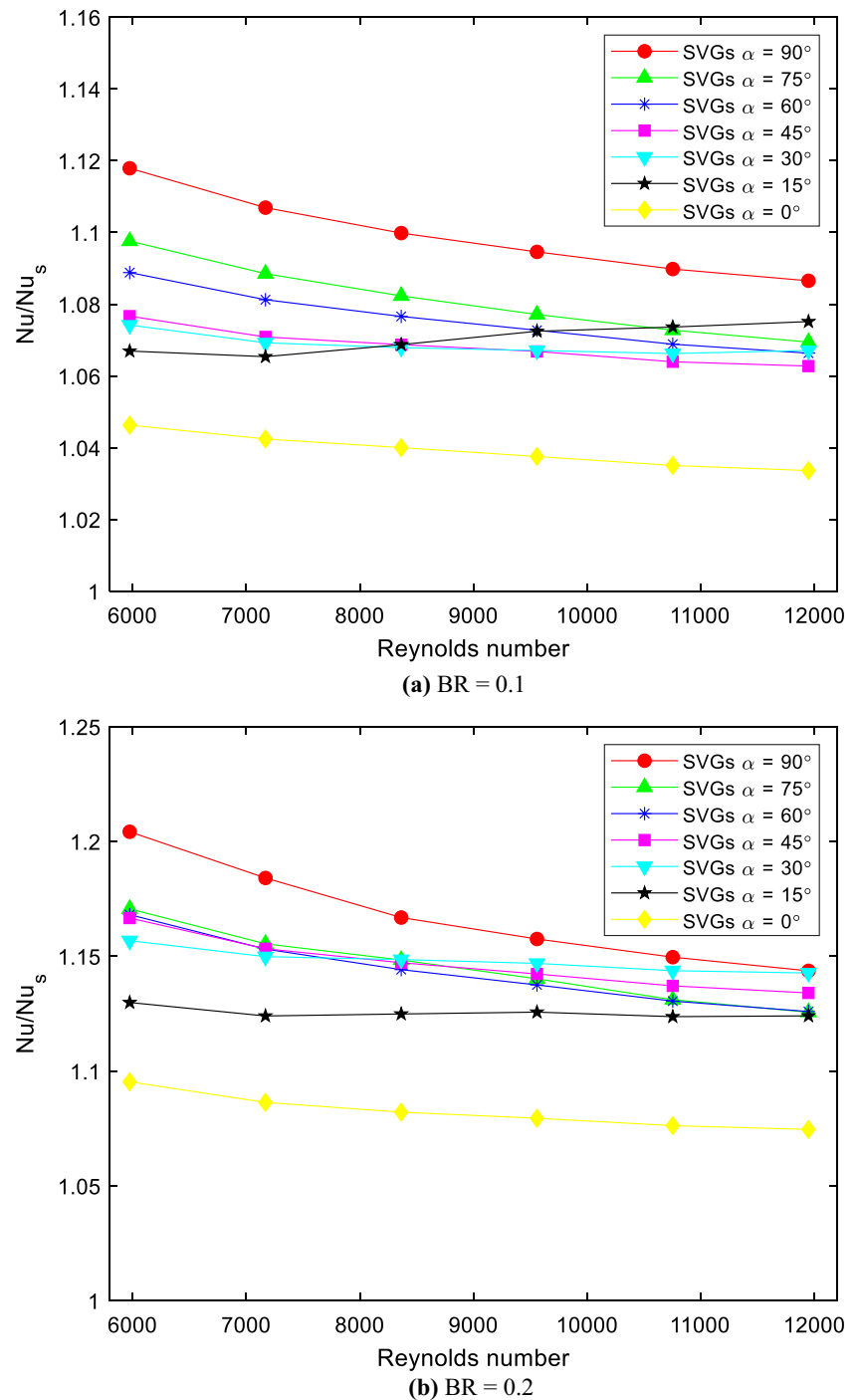
the plain pipe. In contrast, it increases by 14.4% for the case with BR = 0.2, α = 90°, and Re = 11,947.

To understand the vortices evolution along the conduit in detail, the velocity contour and streamlines of the 15° and 45° cases are presented in axial directions with different cross-sections in Fig. 9. Four different locations are selected after the SVG in the flow direction at x of 0.46 m, 0.47 m, 0.55 m, and 0.72 m, where Re and BR were kept at 11,947 and 0.1, respectively. In the 15° case,

four large vortices are observed in different cross-sections within the channel. The vortices originate near the SVG at x = 0.46 m. It became larger and more powerful to mix the flow throughout the domain at x = 0.47 m. At x = 0.55 m, the vortices are smaller, and their centers gradually shift toward the freestream of the flow. These two interacting vortices create a high-pressure zone in between. When the flow reaches the position at x = 0.72 m, the longitudinal vortices diminish in size and strength, resulting in

Fig. 9 Velocity contour and streamlines at different cross-sections of the pipe with SVGs **a** $\alpha = 15°$ and **b** $\alpha = 45°$ at Re = 11,947 and BR = 0.1
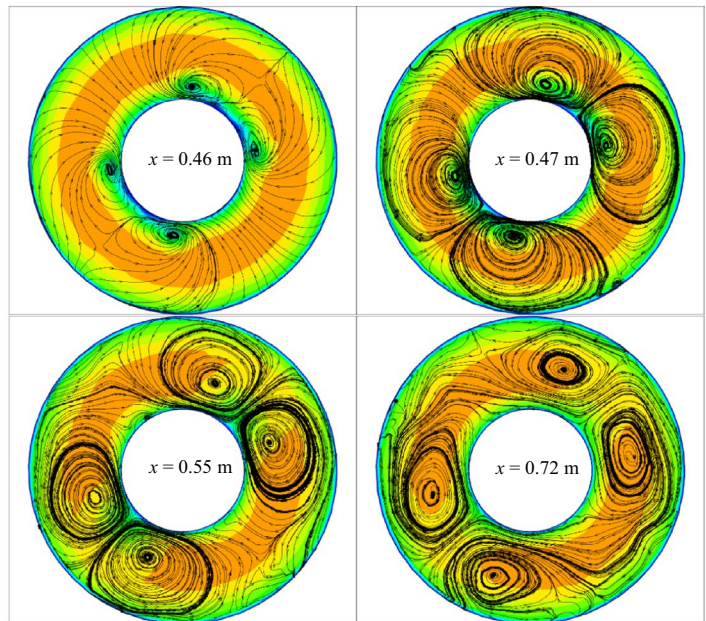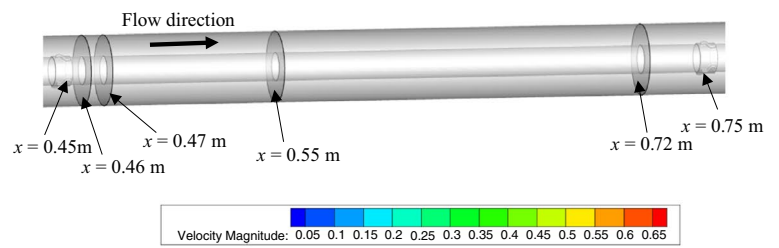
(a) $\alpha = 15°$
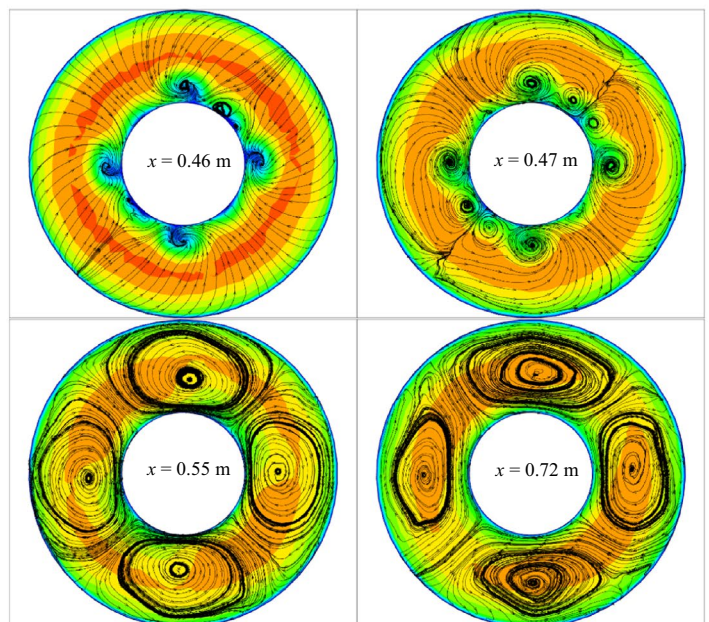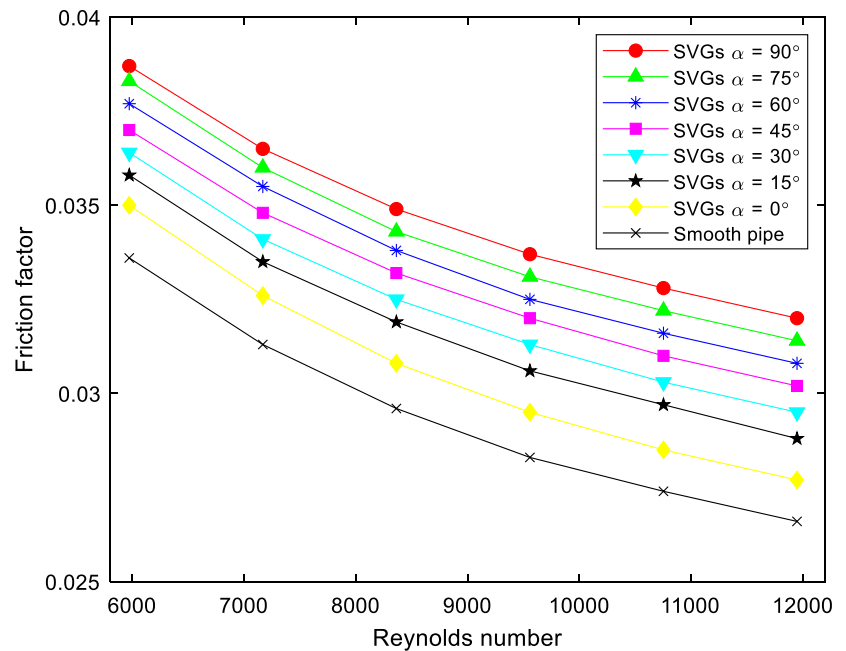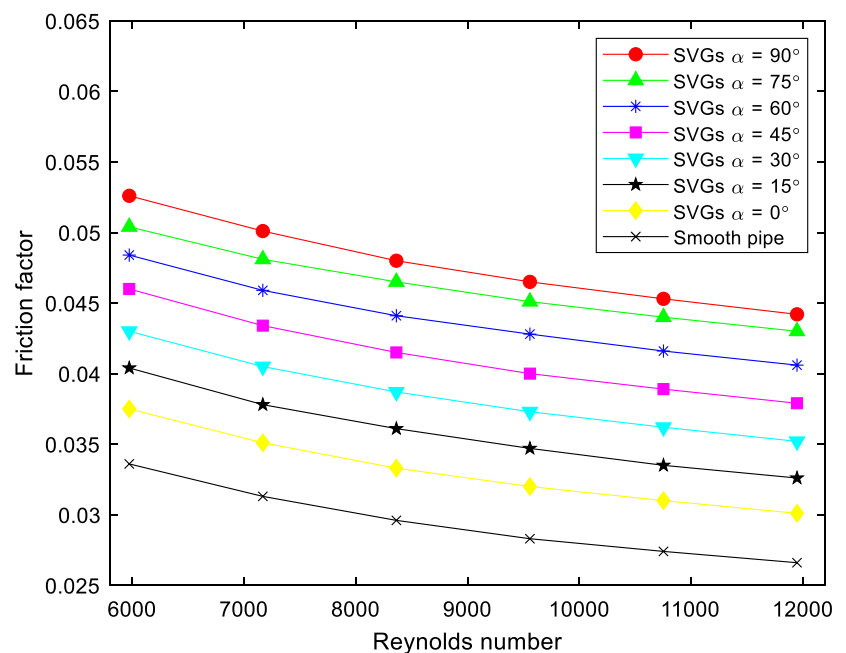
(b) $\alpha = 45°$

Fig. 10 Friction factor variations of various conduits with **a** BR = 0.1 and **b** BR = 0.2
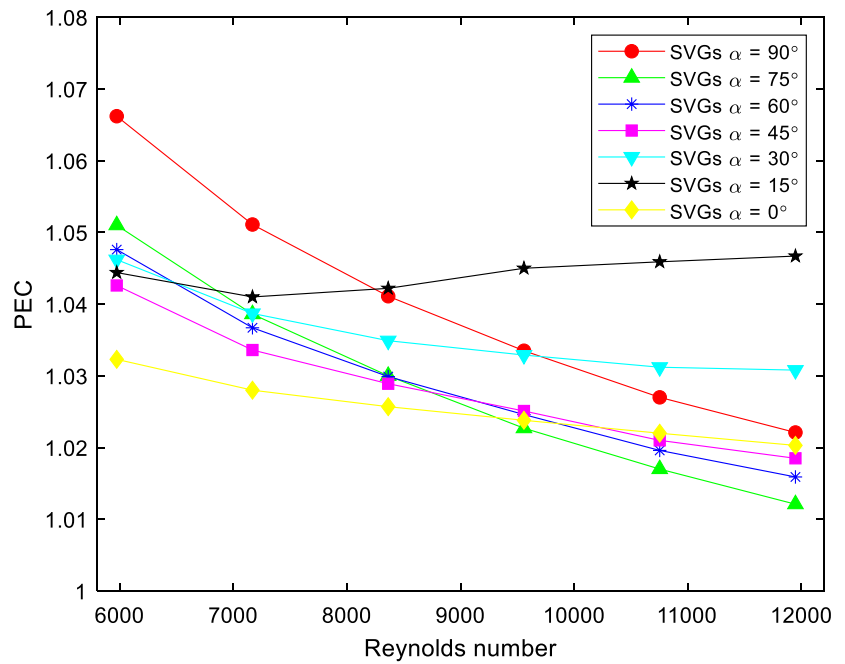

(a) BR = 0.1

(b) BR = 0.2

reduced cooling of the inner wall temperature. However, the 45° case generates four large and four small vortices at $x = 0.46$ m. These small vortices contribute to local fluid mixing near the wall but are less efficient in enhancing heat transfer compared to large vortices. At $x = 0.47$ m, the large vortices are fully developed and capable of mixing the whole fluid domain, while the small vortices weaken the energy of the large vortices due to their opposing directions. Consequently, the vortex velocity shows a significant decrease at $x = 0.55$ m. Furthermore, the 45° case exhibits a wider low-velocity zone compared to the 15° case due to greater displacement between the centers of the two vortices. The closer proximity between the vortices facilitates more effective interaction and fluid mixing. Therefore, the low α cases of 15° and 30° involving

Fig. 11 PEC variations of various conduits with **a** BR = 0.1 and **b** BR = 0.2

(a) BR = 0.1
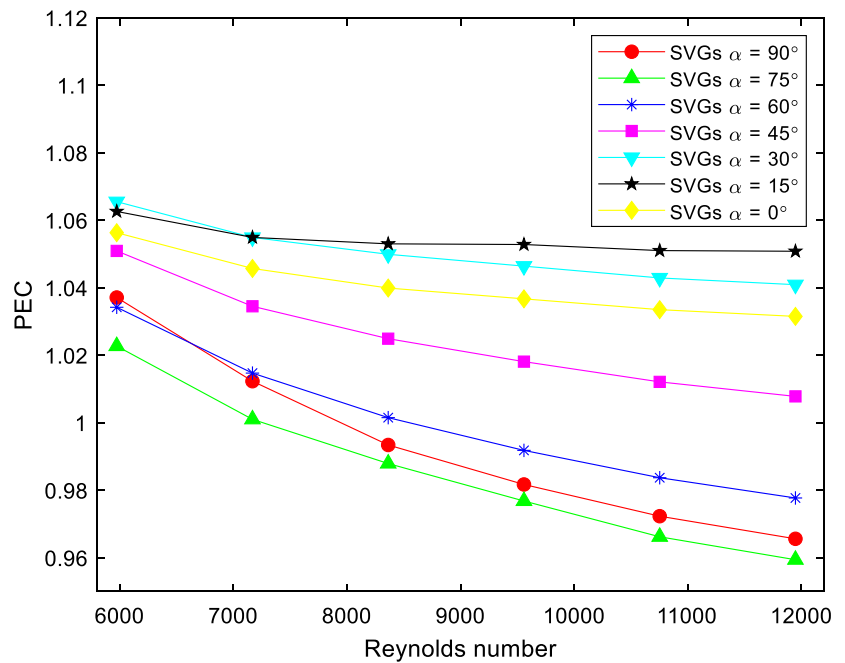
(b) BR = 0.2

consistent prominent vortices tend to perform better as Re increases.

Effects of SVGs on friction factor

Figure 10 shows the friction factor variations of all cases at various Res. The pressure drop is influenced by the friction factor and fluid velocity. All geometries with SVG exhibit a significant increase in friction factor compared to the smooth pipe. The pressure drop increases with the increasing α and BR, as shown in Fig. 6. The case with an α of 90° shows the highest friction factor due to the strong longitudinal and transverse vortices, which are observed in Fig. 4. The friction factor of the model with $\alpha = 90°$, BR = 0.2, and Re = 5973 is 56.5% higher than that of the smooth pipe. In contrast, the lowest friction factor is found in the 0° case, as the pressure drop is generated mainly due to the sinusoidal

shape. The average friction factor improves by only 4% at BR = 0.1 and $\alpha = 0°$ compared to the smooth pipe.

Effects of SVGs on PEC

Figure 11 shows the PEC variations for all cases with various BRs and α. The reference data are the smooth pipe with the PEC value equal to 1. A higher PEC indicates a lower pumping power consumption for better heat transfer at the specific Re. For BR = 0.1, the 90° case shows the highest PEC value when the Re is less than 8363, while the 15° case shows the best PEC when Re is higher than 8363, as explained by the enhanced Nu/Nu_s ratio in Fig. 8. The heat transfer enhancement is more significant than the pressure drop for low α at high Re. Thus, the 15° and 30° cases display better PEC values than other cases when the Re is higher than 9558. For BR = 0.2, cases with smaller α yield better PEC values than those with a larger α. Increasing the height of SVGs reduces the average PEC values for cases with α equal to 60°, 75°, and 90°, and it becomes less than 1 at the high Re. However, applying SVGs could still benefit heat transfer in a certain range of Re. Overall, the case with BR = 0.2 and $\alpha = 15°$ shows the greatest PEC value with an average value of 1.054.

Conclusions

The thermo-hydraulic performance of SVG conduits with BR of 0.1 and 0.2 and α ranging from 0° to 90° has been investigated. By visualizing the flow streamlines, two types of transverse vortices are observed, where one type had its rotational axis normal to the inner pipe surfaces, while the other had its rotational axis parallel to the inner pipe surface. The height of the SVG is crucial in generating the transverse vortices with the axis parallel to the pipe surfaces, while the transverse vortices with the axis perpendicular to the pipe surfaces are affected by the α. Meanwhile, the α and sinusoidal curvature of the SVG is essential in creating the longitudinal vortices. About 0°, 15°, and 30° cases display consistent longitudinal vortices along the channel, while high α cases also produce small vortices. These small longitudinal vortices are inefficient in improving heat transfer as well as the large vortices at high Re. In addition, the pressure drop can be enhanced by raising the height or α of the SVG. The largest Nusselt number augmentation of 20.4% is achieved in the case with BR = 0.2, $\alpha = 90°$, and Re = 5973, while only a 4.6% improvement is observed with BR = 0.1, $\alpha = 0°$, and Re = 5973 when compared to the smooth pipe. Meanwhile, the friction factor increases by 56.5% compared to the smooth tube with BR = 0.2, $\alpha = 90°$, and Re = 5973, while the average friction factor improves by 4% compared

to the smooth pipe when BR = 0.1 and $\alpha = 0°$ are used. The thermo-hydraulic performance decreases with the increased SVG height at higher α due to the increased pressure drop. Overall, the case with BR = 0.1 and $\alpha = 90°$ shows the highest PEC value at Re = 5973, while the case with BR = 0.2 and $\alpha = 15°$ displays the greatest averaged PEC value of 1.054 among all cases.

In addition, there are several works that could be explored in the future studies. The longitudinal vortices are more powerful in cooling the inner wall temperature near the SVGs. The optimized spacing between the SVGs could be investigated to achieve the best thermo-hydraulic performance. Furthermore, the influence of the sinusoidal wave on generating the longitudinal vortices could be optimized by adjusting various parameters of the SVG, such as the magnitude, frequency, and phase. Additionally, the co-rotated arrangement of SVGs can be explored as it causes swirling flow with less pressure drop than the counter-rotated arrangement.

References

1. GandjalikhanNassab SA, Ansari AB, Javaran EJ. Waste heat recovery of exhaust gas in a ribbed double-pipe heat exchanger. Heat Transf Eng. 2022. https://doi.org/10.1080/01457632.2022.2134078.
2. Sadeghi HM, Babayan M, Chamkha A. Investigation of using multi-layer PCMs in the tubular heat exchanger with periodic heat transfer boundary condition. Int J Heat Mass Transf. 2020. https://doi.org/10.1016/j.ijheatmasstransfer.2019.118970.
3. Dogonchi AS, Nayak MK, Karimi N, Chamkha AJ, Ganji DD. Numerical simulation of hydrothermal features of Cu–H_2O nanofluid natural convection within a porous annulus considering diverse configurations of heater. J Therm Anal Calorim. 2020;141(5):2109–25. https://doi.org/10.1007/s10973-020-09419-y.
4. Jawarneh AM, Al-Widyan M, Al-Mashhadani Z. Experimental study on heat transfer augmentation in a double pipe heat

exchanger utilizing jet vortex flow. Heat Transf. 2022;52(1):317–32. https://doi.org/10.1002/htj.22696.

5. Webb RL. Performance evaluation criteria for use of enhanced heat transfer surfaces in heat exchanger design. Int Commun Heat Mass Transf. 1981;24(4):715–26. https://doi.org/10.1016/0017-9310(81)90015-6.

6. Fiebig M. Vortices, generators and heat transfer. Chem Eng Res Des. 1998;76(2):108–23. https://doi.org/10.1205/026387698524686.

7. Arjmandi H, Amiri P, Saffari Pour M. Geometric optimization of a double pipe heat exchanger with combined vortex generator and twisted tape: a CFD and response surface methodology (RSM) study. Therm Sci Eng Prog. 2020. https://doi.org/10.1016/j.tsep.2020.100514.

8. Zhang L, Shang B, Meng H, Li Y, Wang C, Gong B, et al. Effects of the arrangement of triangle-winglet-pair vortex generators on heat transfer performance of the shell side of a double-pipe heat exchanger enhanced by helical fins. Heat Mass Transf. 2016;53(1):127–39. https://doi.org/10.1007/s00231-016-1804-7.

9. Zhang L, Guo H, Wu J, Du W. Compound heat transfer enhancement for shell side of double-pipe heat exchanger by helical fins and vortex generators. Heat Mass Transf. 2012;48(7):1113–24. https://doi.org/10.1007/s00231-011-0959-5.

10. Zhang L, Yan X, Zhang Y, Feng Y, Li Y, Meng H, et al. Heat transfer enhancement by streamlined winglet pair vortex generators for helical channel with rectangular cross section. Chem Eng Process Process Intensif. 2020. https://doi.org/10.1016/j.cep.2019.107788.

11. Mousavi SMS, Alavi SMA. Experimental and numerical study to optimize flow and heat transfer of airfoil-shaped turbulators in a double-pipe heat exchanger. Appl Therm Eng. 2022. https://doi.org/10.1016/j.applthermaleng.2022.118961.

12. El Maakoul A, El Metoui M, Ben Abdellah A, Saadeddine S, Meziane M. Numerical investigation of thermohydraulic performance of air to water double-pipe heat exchanger with helical fins. Appl Therm Eng. 2017;127:127–39. https://doi.org/10.1016/j.applthermaleng.2017.08.024.

13. Wang L, Lei Y, Jing S. Performance of a double-tube heat exchanger with staggered helical fins. Chem Eng Technol. 2022;45(5):953–61. https://doi.org/10.1002/ceat.202100579.

14. Bai W, Chen W, Zeng C, Wu G, Chai X. Thermo-hydraulic performance investigation of heat pipe used annular heat exchanger with densely longitudinal fins. Appl Therm Eng. 2022. https://doi.org/10.1016/j.applthermaleng.2022.118451.

15. Nair SR, Oon CS, Tan MK, Mahalingam S, Manap A, Kazi SN. Investigation of heat transfer performance within annular geometries with swirl-inducing fins using clove-treated graphene nanoplatelet colloidal suspension. J Therm Anal Calorim. 2022;147(24):14873–90. https://doi.org/10.1007/s10973-022-11733-6.

16. Wang Y, Oon CS, Foo J-J, Tran M-V, Nair SR, Low FW. Numerical investigation of thermo-hydraulic performance utilizing clove-treated graphene nanoplatelets nanofluid in an annular passage with perforated curve fins. Results Eng. 2023. https://doi.org/10.1016/j.rineng.2022.100848.

17. Hatami M, Ganji DD, Gorji-Bandpy M. Experimental and thermodynamical analyses of the diesel exhaust vortex generator heat exchanger for optimizing its operating condition. Appl Therm Eng. 2015;75:580–91. https://doi.org/10.1016/j.applthermaleng.2014.09.058.

18. Khoshvaght-Aliabadi M, Akbari MH, Hormozi F. An empirical study on vortex-generator insert fitted in tubular heat exchangers with dilute Cu–water nanofluid flow. Chin J Chem Eng. 2016;24(6):728–36. https://doi.org/10.1016/j.cjche.2016.01.014.

19. Liang G, Islam MD, Kharoua N, Simmons R. Numerical study of heat transfer and flow behavior in a circular tube fitted with varying arrays of winglet vortex generators. Int J Therm Sci. 2018;134:54–65. https://doi.org/10.1016/j.ijthermalsci.2018.08.004.

20. Pourhedayat S, Pesteei SM, Ghalinghie HE, Hashemian M, Ashraf MA. Thermal-exergetic behavior of triangular vortex generators through the cylindrical tubes. Int J Heat Mass Transf. 2020. https://doi.org/10.1016/j.ijheatmasstransfer.2020.119406.

21. Wijayanta AT, Istanto T, Kariya K, Miyara A. Heat transfer enhancement of internal flow by inserting punched delta winglet vortex generators with various attack angles. Exp Thermal Fluid Sci. 2017;87:141–8. https://doi.org/10.1016/j.expthermflusci.2017.05.002.

22. Wijayanta AT, Yaningsih I, Aziz M, Miyazaki T, Koyama S. Double-sided delta-wing tape inserts to enhance convective heat transfer and fluid flow characteristics of a double-pipe heat exchanger. Appl Therm Eng. 2018;145:27–37. https://doi.org/10.1016/j.applthermaleng.2018.09.009.

23. Zhai C, Islam MD, Simmons R, Barsoum I. Heat transfer augmentation in a circular tube with delta winglet vortex generator pairs. Int J Therm Sci. 2019;140:480–90. https://doi.org/10.1016/j.ijthermalsci.2019.03.020.

24. Zhai C, Islam MD, Alam MM, Simmons R, Barsoum I. Parametric study of major factors affecting heat transfer enhancement in a circular tube with vortex generator pairs. Appl Therm Eng. 2019;153:330–40. https://doi.org/10.1016/j.applthermaleng.2019.03.018.

25. Liu H-L, Li H, He Y-L, Chen Z-T. Heat transfer and flow characteristics in a circular tube fitted with rectangular winglet vortex generators. Int J Heat Mass Transf. 2018;126:989–1006. https://doi.org/10.1016/j.ijheatmasstransfer.2018.05.038.

26. Sun Z, Zhang K, Li W, Chen Q, Zheng N. Investigations of the turbulent thermal-hydraulic performance in circular heat exchanger tubes with multiple rectangular winglet vortex generators. Appl Therm Eng. 2020. https://doi.org/10.1016/j.applthermaleng.2019.114838.

27. Abdelmaksoud WA, Mahfouz AE, Khalil EE. Thermal performance enhancement for heat exchanger tube fitted with vortex generator inserts. Heat Transf Eng. 2020;42(21):1861–75. https://doi.org/10.1080/01457632.2020.1826743.

28. Chokphoemphun S, Pimsarn M, Thianpong C, Promvonge P. Heat transfer augmentation in a circular tube with winglet vortex generators. Chin J Chem Eng. 2015;23(4):605–14. https://doi.org/10.1016/j.cjche.2014.04.002.

29. Du J, Hong Y, Huang S-M, Ye W-B, Wang S. Laminar thermal and fluid flow characteristics in tubes with sinusoidal ribs. Int J Heat Mass Transf. 2018;120:635–51. https://doi.org/10.1016/j.ijheatmasstransfer.2017.12.047.

30. Nakhchi ME, Hatami M, Rahmati M. Experimental evaluation of performance intensification of double-pipe heat exchangers with rotary elliptical inserts. Chem Eng Process Process Intensif. 2021. https://doi.org/10.1016/j.cep.2021.108615.

31. Promvonge P, Promthaisong P, Skullong S. Thermal performance augmentation in round tube with louvered V-winglet vortex generator. Int J Heat Mass Transf. 2022. https://doi.org/10.1016/j.ijheatmasstransfer.2021.121913.

32. Rambhad KS, Kalbande VP, Kumbhalkar MA, Khond VW, Jibhakate RA. Heat transfer and fluid flow analysis for turbulent flow in circular pipe with vortex generator. SN Appl Sci. 2021. https://doi.org/10.1007/s42452-021-04664-8.

33. Wang Y, Liu P, Xiao H, Liu Z, Liu W. Design and optimization on symmetrical wing longitudinal swirl generators in circular tube for laminar flow. Int J Heat Mass Transf. 2022. https://doi.org/10.1016/j.ijheatmasstransfer.2022.122961.

34. Wei C, Alexander Vasquez Diaz G, Wang K, Li P. 3D-printed tubes with complex internal fins for heat transfer

enhancement—CFD analysis and performance evaluation. AIMS Energy. 2020;8(1):27–47. https://doi.org/10.3934/energy.2020.1.27.

35. Zheng N, Liu P, Shan F, Liu Z, Liu W. Sensitivity analysis and multi-objective optimization of a heat exchanger tube with conical strip vortex generators. Appl Therm Eng. 2017;122:642–52. https://doi.org/10.1016/j.applthermaleng.2017.05.046.

36. Kumaresan G, Vijayakumar P, Ravikumar M, Kamatchi R, Selvakumar P. Experimental study on effect of wick structures on thermal performance enhancement of cylindrical heat pipes. J Therm Anal Calorim. 2018;136(1):389–400. https://doi.org/10.1007/s10973-018-7842-2.

37. Syam Sundar L, Singh MK, Sousa ACM. Investigation of thermal conductivity and viscosity of Fe_3O_4 nanofluid for heat transfer applications. Int Commun Heat Mass Transf. 2013;44:7–14. https://doi.org/10.1016/j.icheatmasstransfer.2013.02.014.

38. Roache PJ, Knupp PM. Completed Richardson extrapolation. Commun Numer Methods Eng. 1993;9(5):365–74. https://doi.org/10.1002/cnm.1640090502.

39. Gnielinski V. Heat transfer coefficients for turbulent flow in concentric annular ducts. Heat Transfer Eng. 2009;30(6):431–6. https://doi.org/10.1080/01457630802528661.

40. Mozafarie SS, Javaherdeh K, Ghanbari O. Numerical simulation of nanofluid turbulent flow in a double-pipe heat exchanger equipped with circular fins. J Therm Anal Calorim. 2020;143(6):4299–311. https://doi.org/10.1007/s10973-020-09364-w.